PCCP

ROYAL SOCIETY OF CHEMISTRY

PAPER

View Article Online
View Journal | View Issue



Cite this: *Phys. Chem. Chem. Phys.*, 2023, **25**, 13399

# Experimental demonstration of the suppression of viscous fingering in a partially miscible system

Kaori Iwasaki,[a] Yuichiro Nagatsu,[a] Takahiko Ban,[b] Jun Iijima,[a] Manoranjan Mishra[c] and Ryuta X. Suzuki *[ad]

Phase separation is ubiquitous in nature and technology. So far, the focus has primarily been on phase separation occurring in the bulk phase. Recently, phase separation taking place in interfacial areas has attracted more attention – in particular, a combination of interfacial phase separation and hydrodynamics. Studies on this combination have been conducted intensively in this past decade; however, the detailed dynamics remain unclear. Here, we perform fluid displacement experiments, where a less viscous solution displaces a more viscous one in a radially confined geometry and phase separation occurs at the interfacial region. We demonstrate that a finger-like pattern, due to the viscosity contrast during the displacement, can be suppressed by the phase separation. We also claim that the direction of a body force, the so-called Korteweg force, which appears during the phase separation and induces convection, determines whether the fingering pattern is suppressed or changed to a droplet pattern. The change of the fingering pattern to the droplet pattern is enhanced by the Korteweg force directed from the less viscous solution to the more viscous one, whereas the fingering is suppressed by the force directed in the opposite direction. These findings will contribute directly to the higher efficiency of processes such as enhanced oil recovery and $CO_2$ sequestration, where interfacial phase separation is considered to occur during the flow.

Received 26th January 2023,
Accepted 15th April 2023

DOI: 10.1039/d3cp00415e

rsc.li/pccp



## 1 Introduction

Phase separation that takes place in interfacial areas between two phases, such as liquid–liquid phases, where non-premixed phases are brought into contact with each other, has recently attracted considerable research interest; this is in contrast to phase separation that occurs in the bulk phase, which has predominantly been considered so far. Interfacial phase separation has many applications, for example, it is used as a microencapsulation technique through an interfacial phase separation method,[1,2] in the fabrication of flexible, highly porous substrates,[3] and the production of colloidosomes.[4] Yeo *et al.*[1] developed a novel microencapsulation technique that makes use of interfacial mass transfer between mutually soluble liquids, where liquid–liquid phase separation occurs. Allijn *et al.*[3] proposed a one-step method to produce large porous membrane-based scaffolds formed through air–water interfacial phase separation. Zhu *et al.*[4] demonstrated a robust, bottom-up method to produce an all-aqueous hierarchical multicellular structure using interfacial phase separation at the boundary of two non-equilibrium aqueous phases. These studies have facilitated top-down technologies, such as 3D printing, microcapsules, and microfluidics, as well as tissue-engineering applications such as porous membrane-based structures. Such studies are performed based on the interfacial phase separation itself.

Recently, studies on interfacial hydrodynamics combined with interfacial phase separation have been conducted. Examples of the interfacial hydrodynamics considered are Saffman–Taylor instability[5] due to a viscosity contrast, or Rayleigh–Taylor instability[6,7] due to a density difference. Numerical simulations by Hong and Kim[8] have shown that gravitational fingering due to Rayleigh–Taylor instability with interfacial phase separation results in droplets with vertical Hele-Shaw cells. In this paper, we focus on the Saffman–Taylor instability. This instability results in a finger-like pattern when a more viscous fluid is displaced by a less viscous one in a porous medium or in Hele-Shaw cells, wherein two parallel plates are separated by a thin gap. The phenomenon is also called viscous fingering (VF).[9] From the viewpoint of miscibility, the study of VF is classically divided into two categories. The first involves a fully miscible system where two fluids are completely mixed and infinitely mutually soluble,

[a] *Department of Chemical Engineering, Tokyo University of Agriculture and Technology, Naka-cho 2-24-16, Koganei, Tokyo 184-8588, Japan. E-mail: ryuta.x.suzuki@gmail.com*
[b] *Division of Chemical Engineering, Department of Materials Engineering Science, Graduate School of Engineering Science, Osaka University, Machikaneyamacho 1-3, Toyonaka City, Osaka 560-8531, Japan*
[c] *Department of Mathematics, Indian Institute of Technology Ropar, Rupnagar 140001, India*
[d] *PRESTO, Japan Science and Technology Agency, Kawaguchi, Saitama 332-0012, Japan*

resulting in a single phase. In such cases, the dynamics of VF are dominated by diffusion. The other is an immiscible system in which the two fluids do not mix due to a lack of mutual solubility, and thus maintain their initial compositions, where interfacial tension dominates the VF dynamics. Very recently, a third category, namely a partially miscible system, has been studied. A partially miscible system is one in which two fluids initially mix and then separate into two phases over time due to finite mutual solubility. In such a case, the dynamics of VF are initially dominated by diffusion, followed by phase separation. The Saffman–Taylor instability (or VF) with phase separation is an example of interfacial hydrodynamics with interfacial phase separation.

The first study on VF in a partially miscible system was reported by Fu *et al.*,[10] who demonstrated that less viscous $CO_2$ displaces more viscous water in Hele-Shaw cells; they also showed that partial miscibility could control the degree of fingering to a certain extent. In parallel, Amooie *et al.*[11] modelled VF for fully miscible ($CO_2$–oil) and partially miscible ($CO_2$ and $N_2$–oil) systems, and proved that $CO_2$ VF in a partially miscible system is suppressed compared with that in a fully miscible system owing to the interphase mass change leading to a diminished contrast in viscosity. Later on, Suzuki *et al.*[12] showed experimentally that VF in a partially miscible system is qualitatively changed to multiple droplet formation. The origin of this formation is attributed to the nature of phase separation and spontaneous convection induced by the so-called Korteweg force.[13–18] The fingering pattern has also been shown to be induced in partially miscible systems in a viscously stable situation where the more viscous solution displaces the less viscous one in Hele-Shaw cells.[19] Partially miscible systems have also been reported experimentally to show anomalous patterns because of the phase separation.[20,21] Numerical simulations by Seya *et al.*[22] reproduced such multiple-droplet formation with a partially miscible system.

Notably, the Korteweg force in partially miscible systems is different from the so-called Korteweg stress or effective interfacial tension in a fully miscible system, which can be expressed *via* the concentration gradient:[23]

$$\gamma_E = k\int_{-\infty}^{\infty}\left(\frac{dc}{dx}\right)^2 dx \approx k\frac{(\Delta c)^2}{\delta} \quad (1)$$

where $k$ is the Korteweg constant, $c$ is concentration, $\delta$ is interfacial width, and $x$ is the coordinate orthogonal to the interface. The parameter $\gamma_E$ is known as the effective interfacial tension (EIT) and acts as the interfacial tension in immiscible systems. The other interpretation is the aforementioned Korteweg force, which is induced by a chemical potential gradient during phase separation and induces spontaneous convection.[15,24,25] In brief, the Korteweg stress in a fully miscible system is driven by a compositional gradient, whereas the Korteweg force under thermodynamically unstable conditions (spinodal decomposition) is driven by a chemical potential gradient and induces convection. In the present study, we focus on the Korteweg force because we are specifically considering partially miscible systems.

Although interfacial hydrodynamics with phase separation have been studied in the literature, the suppression of VF has not been reported so far. However, technologies for the suppression of such partially miscible VF are essential because of their application in high-pressure and/or high-temperature processes, such as enhanced oil recovery[26] and $CO_2$ sequestration.[27]

There have been many studies on VF suppression in Newtonian fluids with geometry strategies,[28–32] injection control,[33–35] viscoelastic Hele-Shaw cells,[36–38] wettability control,[39] and particle use.[40] Rabaud *et al.*[28] theoretically and experimentally showed that an enforced time-periodic perturbation with the correct frequency dominates the destabilization of viscous fingers. Thomé *et al.*[29] experimentally showed stable VF in sector-shaped cells and not in rectilinear Hele-Shaw cells. Ai-Housseiny *et al.*[30] employed a strategy of gap control, where they inclined the gap at a certain angle and reported that fingering is inhibited with a positive gradient of the cell gap. Numerical simulations by Dias *et al.*[31] reported the suppression of VF with a time-dependent change in cell gap. Zhen *et al.*[32] experimentally demonstrated the suppression of VF with time-dependent gap control. Li *et al.*[33] reported that an immiscible viscous finger could be numerically and experimentally suppressed with a time-dependent injection flow rate. Dias *et al.*[35] theoretically and experimentally showed how an immiscible viscous finger could be controlled using an optimal flow rate, which increases linearly with time in a specific manner. Analogous to the suppression of immiscible VF patterns by lifting Hele-Shaw cells,[31,33,41] Chen *et al.*[34] showed numerically that the same strategy is adaptable to miscible viscous fingers, where the fingers can be inhibited *via* properly controlled injections. The use of viscoelastic Hele-Shaw cells instead of glass plates can experimentally suppress immiscible fingering, which was reported by Pihler-Puzović *et al.*[36–38] Zhao *et al.*[39] experimentally showed that changing the wettability inhibits immiscible VF over a certain threshold value. Tang *et al.*[40] also experimentally demonstrated that the introduction of particles to a less viscous solution during injection can suppress the formation of fingering patterns.

The control of VF through chemical reactions occurring at the interface between two liquids has been studied.[42–51] De Wit and Homsy[42] numerically explored the effect of a chemical reaction on the VF dynamics, where the concentration field obeyed a reaction–convection–diffusion equation in which the rate of chemical reaction was taken to be a function of the concentration of a single chemical species and admitted two stable equilibria separated by an unstable one. They showed that a certain condition provides droplet formation. Nagatsu *et al.*[43] experimentally showed that a chemical reaction inducing a viscosity change at the interface provides sparse or dense patterns of viscous fingers, depending on the product viscosity. Nagatsu *et al.*[44] also experimentally showed that a precipitation reaction made more complex VF patterns. A reaction producing a gel-like material changed from VF to a spiral fingering pattern, which was experimentally reported by Nagatsu *et al.*[51] Moreover, Riolfo *et al.*[45] experimentally and numerically showed the effect of a viscosity change *via* a chemical reaction with a non-Newtonian solution to trigger the interfacial

 

hydrodynamics. Escala *et al.*[47,48,50] designed the contents of each liquid in such a way that a chemical reaction took place at the interface, and they used this reaction to control the fingering instability. However, to the best of our knowledge, there have been no studies on the chemical suppression of VF patterns.

In this paper, we experimentally demonstrate the suppression of VF in a partially miscible system, and we analyse its mechanism by performing additional experimental investigations.

## 2 Experiment

A partially miscible system is achieved at room temperature and atmospheric pressure in a system that consists of poly(ethylene glycol) 8000 (PEG, average molecular weight, $M_w$ = 8000), $Na_2SO_4$, and water.[52] Fig. 1 shows the phase diagram of the solution used. In the present study, 30, 35, 40, and 45 wt% PEG solutions were used for the more viscous solution and a 16 wt% $Na_2SO_4$ solution was used for the less viscous solution. When the initial concentration at the interfacial region between the displacing and displaced liquids falls within the green region in Fig. 1, the system separates into two phases, indicating a partially miscible system. This is because the separation occurs with a finite solubility. In partially miscible systems, the phase separation of the spinodal decomposition type occurs during the fluid displacement. When the initial concentration at the interfacial region is within the blue region, the system exhibits a single phase. This implies a fully miscible system, as the fluids mix completely and form a single phase over time. We assume that the initial concentration at the interfacial region between the displacing and displaced liquids is half the concentration of the two liquids before being in contact with each other. For example, when the displaced liquid is 30 wt% PEG–70 wt% water, and the displacing liquid is 16 wt% $Na_2SO_4$–84 wt% water, the concentration of the mixture of the two liquids is 15 wt% PEG–8 wt% $Na_2SO_4$–77 wt% water (the bottom green point in Fig. 1). This composition is in the green region of Fig. 1 and, thus, the system is partially miscible. For the 35, 40, 45 wt% PEG solutions, the initial concentrations at the interfacial region are shown as other three green points. Therefore, all the prepared solution systems are partially miscible. This assumption is very simple, but we consider it to be appropriate. In a previous study,[12] the same assumption was taken into consideration, and explained by the fact that the results of the fluid displacement, the calculation of free energy, and results of the interfacial tension measurement were all in good agreement. Notably, the more viscous PEG solutions are coloured with 0.1 wt% indigo carmine to visualise the displacement process. The indigo carmine does not dissolve in the $Na_2SO_4$ solution due to the salting-out effect. Therefore, we can track the interface between the PEG-rich and $Na_2SO_4$-rich solutions. Furthermore, the experiments and measurements for the viscosity and interfacial tension shown later are conducted using the solutions dyed with indigo carmine. Hence, we observe the dynamics including the dye in the present study. As the concentration of the $Na_2SO_4$ solution is maintained to be constant for all cases, the viscosity contrast depends on the PEG concentration. The viscosities of the solution used here are measured using a commercial rheometer (AR-G2) from TA-Instruments, Japan, with a cone plate. The viscosity results are shown in Fig. 2, where we measure the shear viscosity against the shear rate. We then found that all solutions are Newtonian because constant values are obtained at all shear rates.

To compare partially miscible systems with immiscible systems, we prepared an immiscible fluid pair. This system consists of phases L and H. An aqueous solution composed of 22.5 wt% PEG and 8 wt% $Na_2SO_4$ (the top green point in Fig. 1) is separated into a PEG-rich phase (phase L, the lighter phase; top red diamond in Fig. 1) and a $Na_2SO_4$-rich phase (phase H, the heavier phase; bottom red diamond in Fig. 1). Phase L is dyed blue with 0.04 wt% indigo carmine. The solution system used here and the physical properties, such as viscosity and density, are summarized in Table 1.

The displacement experiments of the more viscous PEG solutions with various concentrations of the less viscous

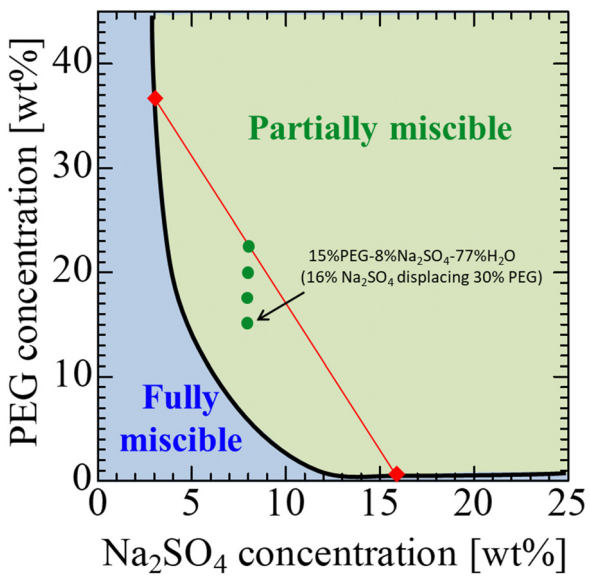


Fig. 1 Phase diagram for a PEG–$Na_2SO_4$–$H_2O$ system.[52] The solid curve shows the binodal curve.

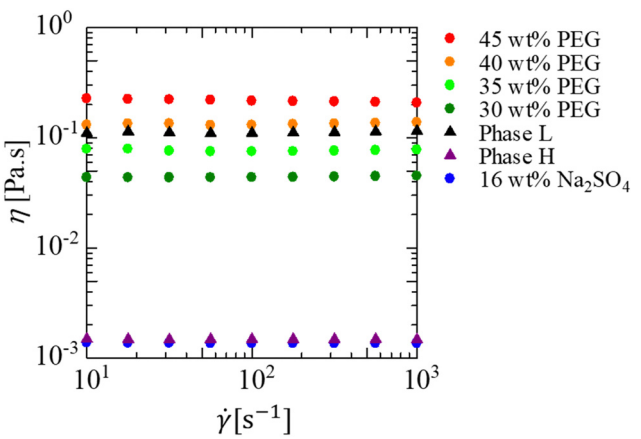


Fig. 2 Shear viscosity measurements.

Table 1 Solution system parameters used here

| Displaced, more viscous solutions (viscosity [mPa s], density [g cm$^{-3}$]) | Displacing, less viscous solutions (viscosity [mPa s], density [g cm$^{-3}$]) |
|---|---|
| 45 wt% PEG solution (217, 1.08) | 16 wt% $Na_2SO_4$ solution (1.36, 1.15) |
| 40 wt% PEG solution (133, 1.07) | |
| 35 wt% PEG solution (76.6, 1.06) | |
| 30 wt% PEG solution (43.9, 1.05) | |
| Phase L (112, 1.06) | Phase H (1.48, 1.14) |

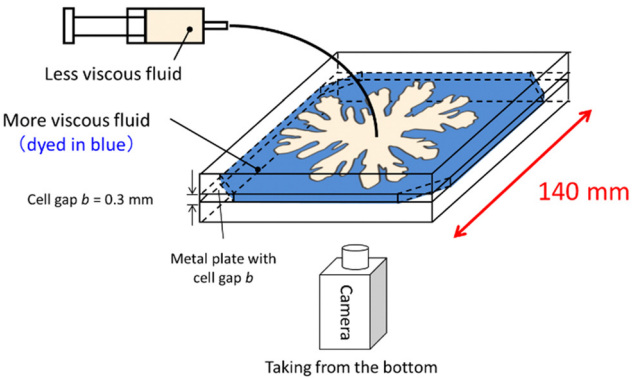


Fig. 3 Schematic of apparatus for VF experiments.

$Na_2SO_4$ solution were conducted using Hele-Shaw cells with a gap of 0.3 mm, as shown in Fig. 3. First, we filled up the cell with the PEG solution, and then injected the $Na_2SO_4$ solution at $9.3 \times 10^{-10}$ m$^3$ s$^{-1}$, controlled using a syringe pump. The displacement experiments were recorded from below the cell using a video camera.

## 3 Results and discussion

The VF experimental results are shown in Fig. 4. The 30 wt% and 35 wt% PEG cases show droplet formation, which is similar to the previous report.[12] Conversely, the 40 wt% PEG case shows a wide fingering pattern. Interestingly, the 45 wt% PEG case shows a circular pattern, where the VF pattern is suppressed. A fingering pattern is obtained for the immiscible system consisting of phases L and H. The time evolution of the representative patterns is shown in Fig. 5. The droplet pattern (Fig. 5(a)) started immediately after the injection was started. Then, more droplets appeared from the center of the injection hole. Conversely, the circular pattern with the suppressed VF (Fig. 5(b)) maintained the circular shape all of the time. By contrast, the typical fingering pattern with phases L and H (Fig. 5(c)) began with a deformed circular shape at first, and then grew into a finger-like pattern.

The droplet pattern has been reported to be induced by the spinodal decomposition type of phase separation and the Korteweg force.[12] As described by Mauri *et al.*[13,53] and Poesio *et al.*,[14] a force produced under spinodal decomposition is referred to as the Korteweg force. This is thermodynamically defined as the functional derivative of the free energy[53] and is characterized by a body force. This force produces spontaneous convection to minimize the free energy stored at the interface;[13–18,53] in addition, it has been reported that droplets can move spontaneously due to the Korteweg force.[13–18] The first experimental study and numerical simulation of such droplet formation with a partially miscible VF pattern were reported by Suzuki *et al.*[12] and Seya *et al.*,[22] respectively. The mechanism of droplet formation clarified in each study is the same: their experimental system undergoes thermodynamic instability and phase separation of a spinodal type. In contrast to normal diffusion, such phase separation promotes mass transfer against the concentration gradients and enhances concentration fluctuations, leading to the separation of the system into low- and high-concentration regions. Furthermore, the body force generated by the chemical potential gradient creates a spontaneous convection, promoting phase separation.[15,54] Thus, the growth of the deformed region due to hydrodynamic instabilities (viscous fingering) is enhanced by the thermodynamic instabilities (phase separation) when the less viscous solution is in contact with the more viscous solution in the spinodal region. Eventually, droplets are detached from the deformed region.

The circular pattern with suppressed VF in partially miscible systems has not been reported so far. First, we consider the mechanism from the viewpoint of a hydrodynamic effect, *i.e.*, a viscosity contrast, which is the origin of the Saffman–Taylor instability. According to the study on the Saffman–Taylor instability in the radial geometry by Paterson,[55] the most

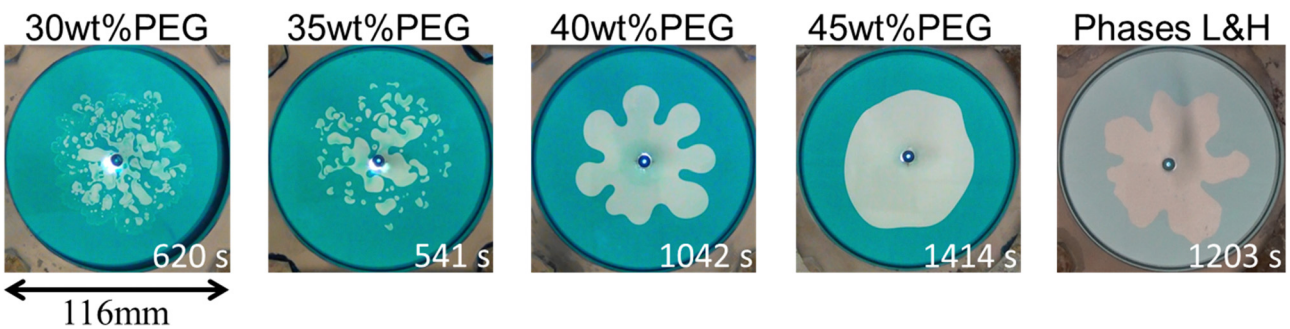


Fig. 4 Patterns obtained by the displacement of a more viscous solution by a less viscous one. The time shown in the bottom right of each image is when the longest finger or droplet reaches 42 mm.

 

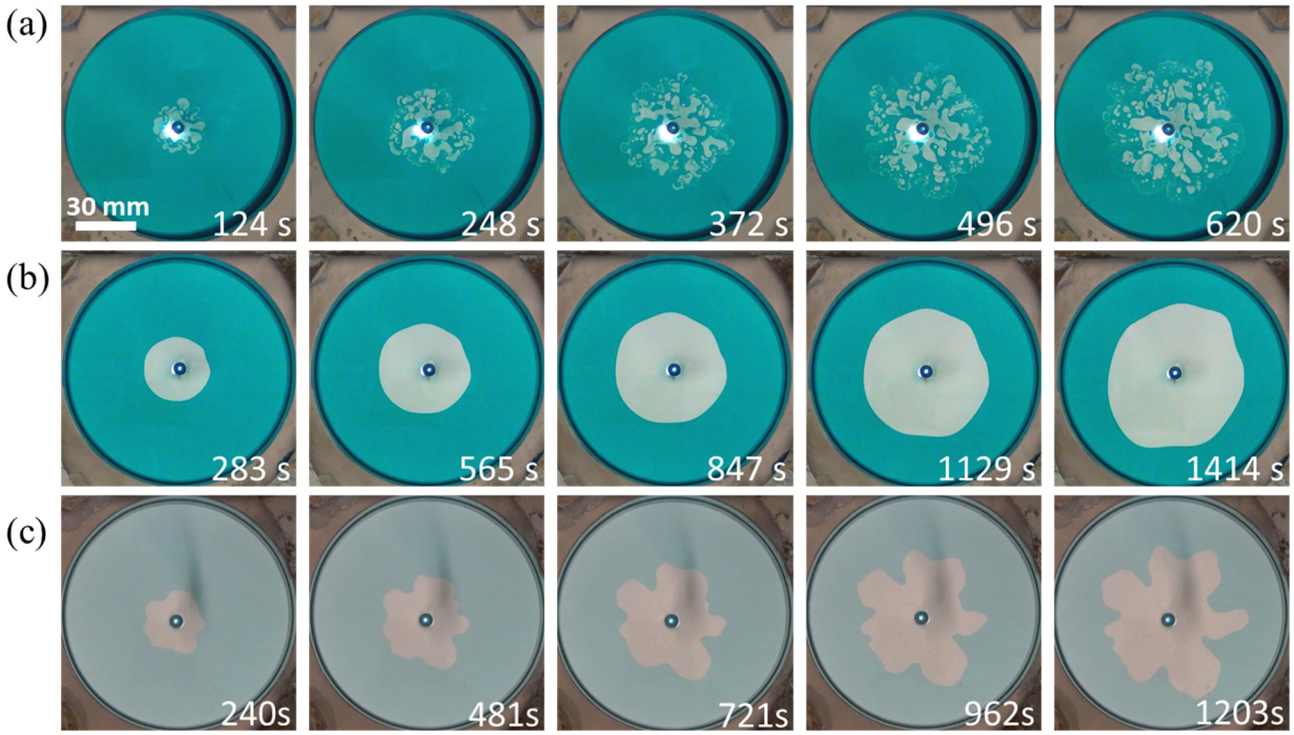


Fig. 5 Time evolution of (a) the droplet pattern, where the PEG concentration is 30 wt%, (b) the pattern with suppressed VF, where the PEG concentration is 45 wt%, and (c) the standard fingering pattern with phases L and H.

rapidly growing linearly unstable wavelength $\lambda_m$ of an interface of radius $r$ is

$$\lambda_m = \frac{2\sqrt{3}\pi r}{\sqrt{\frac{Qr}{2\pi\gamma M_2}+1}} \quad (2)$$

where $r$ [m] is the radius, $Q$ [m$^2$ s$^{-1}$] is the flow rate, $M_2 = b^2/12\eta_{more}$ is the mobility of the more viscous solution (where $\eta$ [Pa s] is the viscosity and $b$ [m] is the gap between cells), and $\gamma$ [N m$^{-1}$] is the interfacial tension. Eqn (2) indicates that $\lambda_m$ becomes smaller when the viscosity of the more viscous solution $\eta_{more}$ is larger, which indicates that more fingers appear when $\eta_{more}$ is larger. Therefore, one can understand that more fingers appear, or that the system becomes hydrodynamically more unstable when the viscosity contrast is larger. The measured viscosity contrast in the present study is as follows: $M_{30wt\%} = (\eta_{more}/\eta_{less}) = 32.3$, $M_{35wt\%} = 56.3$, $M_{40wt\%} = 97.8$, $M_{45wt\%} = 160$, $M_{LH} = 75.7$ for the 30, 35, 40, and 45 wt% PEG cases and the case of phases L and H, respectively. The viscosity contrast for the 45 wt% PEG case is much larger than that of phases L and H, where no chemically thermodynamic effects exist because the system is at equilibrium. Since a larger viscosity contrast leads to a more developed VF pattern, the pattern with suppressed VF for the 45 wt% PEG case cannot be explained from the viewpoint of the viscosity contrast.

Subsequently, we consider the mechanism from the viewpoint of the interfacial energy. The interfacial energy is related to the interfacial tension, and is defined as the first derivative of interfacial energy with respect to the interfacial area. We measure the interfacial tension because the interfacial energy is caused by a chemical thermodynamic effect related to the occurrence of the Korteweg force, as mentioned in the preceding paragraph. In the present study, the time evolution of the interfacial tension was measured with a spinning drop tensiometer[56,57] (SITE100), from KRÜSS, Germany. In Fig. 6 we show the interfacial tension measured *via* the spinning method, which is denoted as $\gamma_m$, where the subscript "m" indicates "measured". The previous report showed that the temporal increase in interfacial tension was evidence for the occurrence of the Korteweg force.[12,19,20]

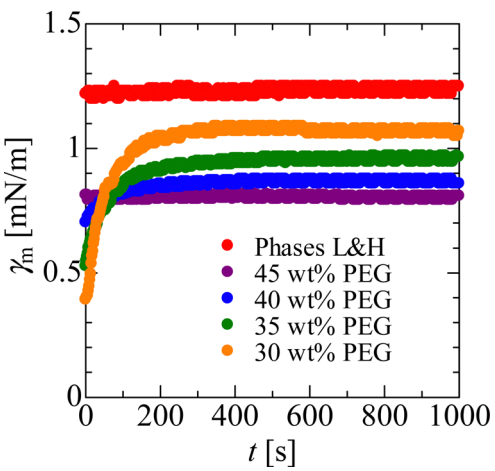


Fig. 6 Time evolution of tmeasured interfacial tension, $\gamma_m$. The measurements are carried out under the conditions of 6000 rpm.

In Fig. 6, a temporal increase in $\gamma_m$ can be observed in the 30–40 wt% PEG cases, and the $\gamma_m$ values are almost constant with time for the 45 wt% PEG case and the case with phases L and H. Therefore, the Korteweg force should occur in the 30–40 wt% PEG case. A constant $\gamma_m$ against time is reasonable for the case of the L and H phases because the system is at equilibrium, implying that such a chemically thermodynamic effect cannot be induced. Although the $\gamma_m$ value for the 45 wt% PEG case does not increase, we consider the temporary increase in genuine interfacial tension and show in the following paragraph that, in this case, the Korteweg force works to suppress the fingering pattern. The reason for the constant $\gamma_m$ despite the temporal increase in the genuine interfacial tension will be discussed in the third to last paragraph of this section.

In addition to the discussion about the interfacial energy, we can discuss another hydrodynamic effect, *i.e.*, the absolute value of the interfacial tension. Based on eqn (2), it is understood that, as the interfacial tension increases under a given viscosity contrast, a more circular pattern is obtained. For this section we employ the interfacial tension measured at equilibrium because the magnitude relationship of the values does not change. From Fig. 6, the equilibrium $\gamma_m$ values obtained are: $\gamma_{30wt\%}$ = 1.07 mN m$^{-1}$, $\gamma_{35wt\%}$ = 0.960 mN m$^{-1}$, $\gamma_{40wt\%}$ = 0.867 mN m$^{-1}$, $\gamma_{35wt\%}$ = 0.802 mN m$^{-1}$, $\gamma_{LH}$ = 1.24 mN m$^{-1}$, where the subscripts denote the respective PEG and L and H cases. The case of the equilibrium L and H phases shows the highest $\gamma_m$ value of all. Therefore, the circular pattern observed with suppressed VF for the 45 wt% PEG case is not caused solely by the hydrodynamic effect of interfacial tension. The pattern with the suppressed VF is caused by a chemical thermodynamic effect.

As discussed above, the pattern with suppressed VF should be caused by the Korteweg force. We now discuss the occurrence and direction of the force. In order to check the occurrence and direction of the Korteweg force, a static experiment was performed. We first filled the Hele-Shaw cell with the less viscous solution (16 wt% $Na_2SO_4$ solution or phase H) and then injected the more viscous solution (PEG solution of several concentrations or phase L) at a high-speed injection rate of 8.2 × 10$^{-9}$ m$^3$ s$^{-1}$ to avoid occurrence of phase separation before our observation. In this experiment, therefore, no interfacial instability during the injection occurred because of the hydrodynamically stable situation, where the more viscous PEG solution (coloured in blue) displaces the less viscous $Na_2SO_4$ solution (colourless and transparent) in the Hele-Shaw cells. After the radius of the more viscous solution reached 20 mm, the injection was stopped, and we observed the behaviour of the pattern. We called this experiment the "stop experiment". The results of the stop experiment are shown in Fig. 7, where the time evolution of the circular interface is displayed for each case. For the 30 and 35 wt% PEG cases, the droplets go into the coloured PEG solution, which indicates that the Korteweg force works from the $Na_2SO_4$ solution to the PEG solution. This direction is consistent with what was reported in previous studies.[19] For the 40 and 45 wt% PEG cases, by contrast, the PEG solution moves outwards. Thus, the direction is opposite to that of the 30 and 35 wt% PEG cases. It is noted that the case of the L and H phases shows no change at the interface because the

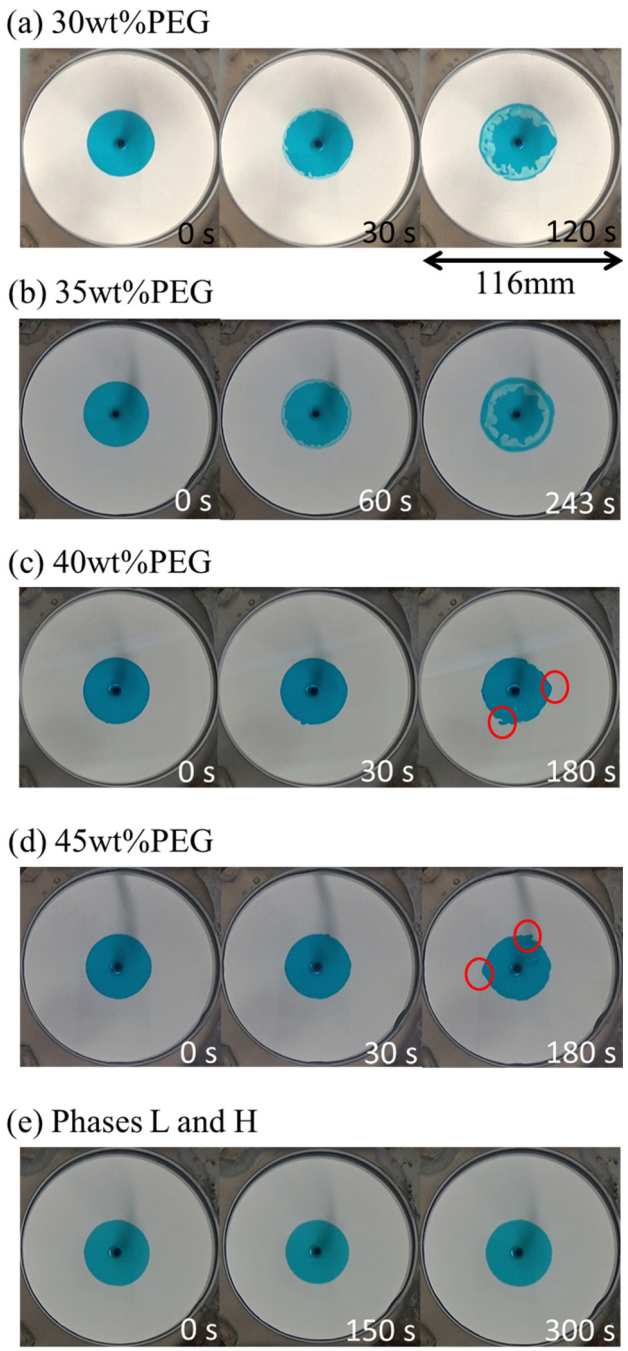


Fig. 7 Time evolution of the interface behavior after stopping the injection of PEG solution into the 16 wt% $Na_2SO_4$ solution. The time in the bottom right of each image indicates when the picture was taken. The red circles show points where the colored PEG solution moved to the $Na_2SO_4$ solution side.

Korteweg force does not exist. As shown in Fig. 6, the interfacial tension changes during the first 200–300 seconds after the two solutions contact each other and reach saturation. The change in the interface behaviour shown in Fig. 7 corresponds to the change in interfacial tension in terms of the time scale. Namely, the deformation of the interface in all the systems except for the phases L and H system (Fig. 7(e)), started within $t$ = 180 s.

 

We observed that the deformation is not saturated over 300 s in the stop experiment. This is probably because the volume ratio of the PEG solution and the $Na_2SO_4$ solution is different between the stop experiment and the spinning drop measurement. We emphasize that the results of the stop experiment show direct experimental demonstration of the meaning of the Korteweg force because we can consider the meaning of the Korteweg force as the force generated during phase separation that causes convection. Therefore, the direction of the Korteweg force plays a key role in determining whether the resulting pattern is characterized by droplets or a suppressed viscous fingering pattern. The Korteweg force for a binary system of species A and B is expressed by:[12,15,18,58,59]

$$F = \left(\frac{\rho RT}{M_w}\right)\tilde{\mu}\nabla\phi \sim -\left(\frac{\rho RT}{M_w}\right)\phi\nabla\tilde{\mu} \quad (3)$$

where $\rho$ is the mixture mass density, $R$ is the gas constant, $T$ is the absolute temperature, $M_w$ is the molecular weight of species of $A$ and $B$, $\tilde{\mu} = \mu_A - \mu_B$ is the chemical potential difference in the mixture, and $\phi$ is the molar fraction. Therefore, the direction of the force can be changed *via* the gradient of $\phi$ or $\tilde{\mu}$. In the present study, we can change the sign of eqn (3) by changing the chemical potential gradient.

In the VF experiments, the injection is directed from $Na_2SO_4$ to PEG. In the 30 and 35 wt% PEG cases, where the Korteweg force is directed from $Na_2SO_4$ to PEG, the direction of the injection and the Korteweg force are aligned, leading to an increased tendency for the fingertips to pinch-off. This promotes the formation of numerous droplets, as mentioned earlier (the second paragraph in this section). Conversely, in the 40 and 45 wt% PEG cases, where the Korteweg force is directed from PEG to $Na_2SO_4$, the injection and the Korteweg force directions are opposite, resulting in a stable interface that produces a circular pattern with suppressed viscous fingering. The explanation for this is described in the next paragraph.

In the following paragraph, we will demonstrate that the stabilization of VF depends not only on the Korteweg force pointing from PEG to $Na_2SO_4$ but also on the interfacial region being thinner at the fingertip compared with the root of the finger. The schematic for the targeted VF is shown in Fig. 8, where the $Na_2SO_4$ solution is injected from left to right. When a finger grows (Fig. 8(a)), the interfacial width between the $Na_2SO_4$ and PEG solutions will become smaller at the fingertip than at its root, owing to larger convection at the fingertip. The Korteweg force is induced by a chemical potential gradient ($\nabla\mu = \Delta\mu/\delta$: where $\Delta\mu$ is the chemical potential difference between the more and less viscous solutions and $\delta$ is the interface width).[15,60] Therefore, the Korteweg force should be larger at the fingertip than at the root because the gradient is larger at the fingertip than at the root. When the Korteweg force is aligned with the flow, it primarily affects the fingertip and enhances the growth of the finger, as shown in Fig. 8(b). Note that, in this case, the finger becomes a droplet due to the nature of phase separation that leads to the pinching-off of the growing fingertip from the mother finger. When the Korteweg force works against the flow, it suppresses the growth of the finger since it works more significantly at the fingertip, as shown in Fig. 8(c).

We here note the reason why the measured interfacial tension, $\gamma_m$, for the 45 wt% PEG case in the spinning drop tensiometer does not increase, although the Korteweg force works to suppress the fingering pattern. The method of the

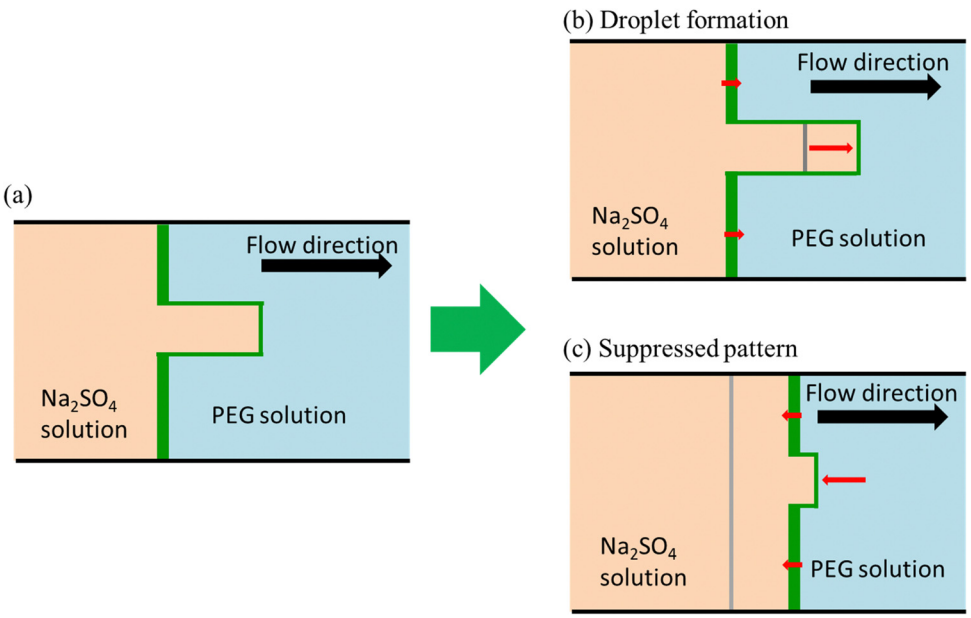


Fig. 8 Schematic of the targeted VF for an explanation of the suppression, where the situations for (a) a growing finger, (b) droplet formation and (c) a suppressed pattern are illustrated. The orange and blue areas show the $Na_2SO_4$ and PEG solutions, respectively. The green line indicates the interface and, thus, the width of the line corresponds to the interface length. The red arrows show the direction of the Korteweg force, and the arrow length corresponds the magnitude of the force.

spinning drop tensiometer is first explained in Fig. 9(a). Vonnegut[61] derived a well-known expression for simple calculation of the interfacial tension $\gamma$, namely:

$$\gamma = \frac{(\rho_1 - \rho_2)\omega^2 R^3}{4}$$

where $\rho_1$ and $\rho_2$ are the heavier and lighter fluid densities, respectively, $\omega$ is the rotational speed, and $R$ is the radius of the droplet in the direction perpendicular to the axis of rotation. The method measures $R$ against time under the condition where $\rho_1$, $\rho_2$ and $\omega$ are constant to obtain the value of the interfacial tension. In the present study, the surrounding heavier solution in Fig. 9(a) is the 16 wt% $Na_2SO_4$ solution or phase H, and the droplet is the PEG solution or phase L. It is understood that the interfacial tension value of a partially miscible system with phase separation increases against time.[12] When the droplet is 30 wt% PEG solution, the direction of the Korteweg force goes from $Na_2SO_4$ to PEG. Hence, the droplet is pushed on both sides in the horizontal direction, resulting in more enhancement to increase $R$. This evidence is shown in Fig. 9(b). By contrast, when the droplet is 45 wt% PEG solution, the direction of the Korteweg force is from PEG to $Na_2SO_4$. The droplet is, therefore, stretched to both sides in the horizontal direction, resulting in a decrease in $R$, which can be observed in Fig. 9(c). However, the $\gamma_m$ value is almost constant against time, even when the droplet stretches. This should be the evidence for increasing of the genuine interfacial tension in the 45 wt% PEG solution case. To summarize, it can be concluded that (i) in the case of 45 wt% PEG, the genuine interfacial tension is increased (thus, the Korteweg force works) despite $\gamma_m$ remaining constant over time, and (ii) in the case of 30 wt% PEG, the genuine interfacial tension is expected to temporally increase because the Korteweg force actually works in the stop experiment. The temporal increase in $\gamma_m$ shown in Fig. 6 can be larger than that in the genuine interfacial tension.

One may consider the third dimension (gap) ($z$-direction) effects on the Hele-Shaw experiment from the interfacial constraint observed in the spinning drop experiments. Therefore, we mention here the third dimension (gap) effects on the Hele-Shaw experiment. In fully miscible systems, these effects have often been reported along with observation of the shade of the dye.[62–66] Conversely, the effects are rarely discussed in immiscible systems, wherein almost no dye shading is observed. Similarly, in the present pattern with suppressed VF, no significant dye shading is observed. Therefore, we consider that third dimension (gap) effects are not observed in the pattern with suppressed VF. In addition, stabilization can be explained in the two-dimensional ($xy$ direction) mode as described in Fig. 8. Based on this argument, we consider that the third dimension (gap) ($z$-direction) effects may not be crucial to the stabilization of VF in the partially miscible system.

Although the present study can contribute to the understanding of $CO_2$-EOR (Enhanced Oil Recovery) because the situation under the ground is thermodynamically similar to this study, considerable research is required to improve the oil recovery efficiency and predict the amount of $CO_2$ able to be injected into the reservoir as the effect of porosity and/or wettability on partially miscible VF patterns is still not clear from this study. Therefore, it will be interesting to incorporate these effects with our current experimental study in the future to fully understand the flow dynamics in partially miscible systems.

## 4 Conclusions

We experimentally demonstrate that the direction of the Korteweg force from a more viscous fluid to a less viscous fluid explains the circular pattern with suppressed VF in partially miscible systems as well as the mechanism for the suppression of VF. There have been many studies on VF suppression through hydrodynamic effects, such as changing the geometry,

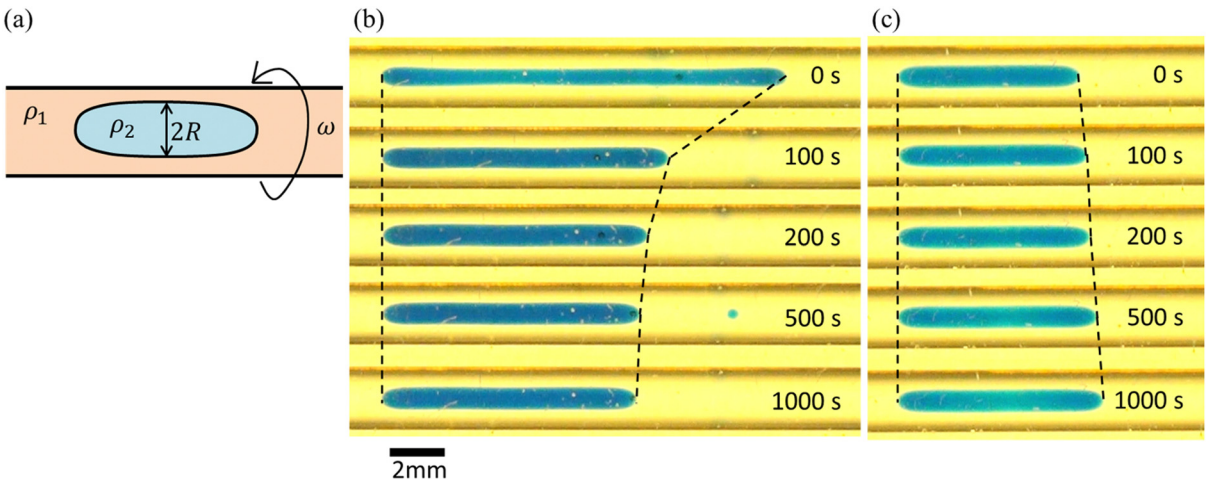


Fig. 9 (a) Schematic of the spinning drop method for interfacial tension measurement. (b) and (c) Time evolution of a droplet during the spinning method for the 16 wt% $Na_2SO_4$–30 wt% PEG system (b), and 16 wt% $Na_2SO_4$–45 wt% PEG system (c). In (b) and (c), the droplet dyed blue is the PEG solution surrounded by the $Na_2SO_4$ solution.

 

time-dependent gap strategies, time-dependent injection strategies and so on; however, the present study demonstrates the first experiment to suppress VF patterns using a chemical strategy in which we change the direction of the chemically thermodynamic Korteweg force. Therefore, the present study can provide new experimental findings on the coupling of interfacial phase separation and interfacial hydrodynamics. These findings will contribute directly to the higher efficiency of processes such as enhanced oil recovery[26] and $CO_2$ sequestration,[27] where interfacial phase separation is considered to occur during the flow.

## Author contributions

K. Iwasaki: investigation, resources, data curation, validation. Y. Nagatsu: conceptualization, methodology, writing – review and editing. T. Ban: methodology, writing – review and editing. J. Iijima: data curation. M. Mishra: methodology, writing – review and editing. R. X. Suzuki: conceptualization, data curation, writing – original draft, writing – review and editing, funding acquisition, supervision, project administration.

## Conflicts of interest

There are no conflicts to declare.

## Acknowledgements

This study is supported by JSPS KAKENHI Grant No. 22K20402 and 22K03900, and JST Presto Grant No. JPMJPR22O5. The authors appreciate Mr Shoji Seya, Tokyo University of Agriculture and Technology, for his assistance in several experiments and fruitful discussions.

## References

1 Y. Yeo, O. A. Basaran and K. Park, A new process for making reservoir-type microcapsules using ink-jet technology and interfacial phase separation, *J. Controlled Release*, 2003, **93**, 161–173.
2 C. Snider, S. Y. Lee, Y. Yeo, G. J. Grégori, J. P. Robinson and K. Park, Microenvironment-controlled encapsulation (MiCE) process: Effects of PLGA concentration, flow rate, and collection method on microcapsule size and morphology, *Pharm. Res.*, 2008, **25**, 5–15.
3 I. Allijn, N. du Preez, M. Tasior, R. Bansal and D. Stamatialis, One-Step Fabrication of Porous Membrane-Based Scaffolds by Air-Water Interfacial Phase Separation: Opportunities for Engineered Tissues, *Membranes*, 2022, **12**, 453.
4 S. Zhu, J. Forth, G. Xie, Y. Chao, J. Tian, T. P. Russell and H. C. Shum, Rapid Multilevel Compartmentalization of Stable All-Aqueous Blastosomes by Interfacial Aqueous-Phase Separation, *ACS Nano*, 2020, **14**, 11215–11224.
5 P. G. Saffman and G. Taylor, The Penetration of a Fluid into a Porous Medium or Hele-Shaw Cell Containing a More Viscous Liquid, *Proc. R. Soc. London, Ser. A*, 1958, **245**, 312–329.
6 L. Rayleigh, Investigation of the Character of the Equilibrium of an Incompressible Heavy Fluid of Variable Density, *Proc. London Math. Soc.*, 1882, **14**, 170–179.
7 D. J. Lewis, The Instability of Liquid Surfaces when Accelerated in a Direction Perpendicular to their Planes. II, *Proc. R. Soc. London, Ser. A*, 1950, **202**, 81–96.
8 J. S. Hong and M. C. Kim, Gravitational fingering and droplet formation during the phase separation of a partially miscible binary mixture in a vertical Hele-Shaw cell, *Int. J. Heat Mass Transfer*, 2023, **201**, 123665.
9 G. M. Homsy, Viscous Fingering in Porous Media, *Annu. Rev. Fluid Mech.*, 1987, **19**, 271–311.
10 X. Fu, L. Cueto-Felgueroso and R. Juanes, Viscous fingering with partially miscible fluids, *Phys. Rev. Fluids*, 2017, **2**, 104001.
11 M. A. Amooie, M. R. Soltanian and J. Moortgat, Hydrothermodynamic mixing of fluids across phases in porous media, *Geophys. Res. Lett.*, 2017, **44**, 3624–3634.
12 R. X. Suzuki, Y. Nagatsu, M. Mishra and T. Ban, Phase separation effects on a partially miscible viscous fingering dynamics, *J. Fluid Mech.*, 2020, **898**, A11.
13 D. Molin, R. Mauri and V. Tricoli, Experimental evidence of the motion of a single out-of-equilibrium drop, *Langmuir*, 2007, **23**, 7459–7461.
14 P. Poesio, G. P. Beretta and T. Thorsen, Dissolution of a liquid microdroplet in a nonideal liquid-liquid mixture far from thermodynamic equilibrium, *Phys. Rev. Lett.*, 2009, **103**, 064501.
15 N. Vladimirova, A. Malagoli and R. Mauri, Diffusiophoresis of two-dimensional liquid droplets in a phase-separating system, *Phys. Rev. E: Stat. Phys., Plasmas, Fluids, Relat. Interdiscip. Top.*, 1999, **60**, 2037–2044.
16 T. Ban, A. Aoyama and T. Matsumoto, Self-generated Motion of Droplets Induced by Korteweg Force, *Chem. Lett.*, 2010, **39**, 1294–1296.
17 T. Ban, T. Yamada, A. Aoyama, Y. Takagi and Y. Okano, Composition-dependent shape changes of self-propelled droplets in a phase-separating system, *Soft Matter*, 2012, **8**, 3908–3916.
18 T. Ban, T. Fukuyama, S. Makino, E. Nawa and Y. Nagatsu, Self-Propelled Vesicles Induced by the Mixing of Two Polymeric Aqueous Solutions through a Vesicle Membrane Far from Equilibrium, *Langmuir*, 2016, **32**, 2574–2581.
19 R. X. Suzuki, Y. Nagatsu, M. Mishra and T. Ban, Fingering pattern induced by spinodal decomposition in hydrodynamically stable displacement in a partially miscible system, *Phys. Rev. Fluids*, 2019, **4**, 104005.
20 R. X. Suzuki, R. Takeda, Y. Nagatsu, M. Mishra and T. Ban, Fluid Morphologies Governed by the Competition of Viscous Dissipation and Phase Separation in a Radial Hele-Shaw Flow, *Coatings*, 2020, **10**, 960.
21 R. X. Suzuki, H. Tada, S. Hirano, T. Ban, M. Mishra, R. Takeda and Y. Nagatsu, Anomalous patterns of Saffman-

Taylor fingering instability during a metastable phase separation, *Phys. Chem. Chem. Phys.*, 2021, **23**, 10926–10935.
22 S. Seya, R. X. Suzuki, Y. Nagatsu, T. Ban and M. Mishra, Numerical study on topological change of viscous fingering induced by a phase separation with Korteweg force, *J. Fluid Mech.*, 2022, **938**, A18.
23 D. Truzzolillo, S. Mora, C. Dupas and L. Cipelletti, Off-equilibrium surface tension in colloidal suspensions, *Phys. Rev. Lett.*, 2014, **112**, 128303.
24 J. E. Farrell and O. T. Valls, Spinodal decomposition in a two-dimensional fluid model, *Phys. Rev. B: Condens. Matter Mater. Phys.*, 1989, **40**, 7027–7039.
25 T. Ban, T. Yamada, A. Aoyama, Y. Takagi and Y. Okano, Composition-dependent shape changes of self-propelled droplets in a phase-separating system, *Soft Matter*, 2012, **8**, 3908–3916.
26 L. W. Lake, R. T. Johns, W. R. Rossen and G. A. Pope, *Fundamentals of Enhanced Oil Recovery*, Society of petroleum engineers, Richardson, TX, 2014.
27 F. M. J. Orr and J. J. Taber, Use of Carbon Dioxide in Enhanced Oil Recovery, *Science*, 1984, **224**, 563–569.
28 M. Rabaud, Y. Couder and N. Gerard, Dynamics and stability of anomalous Saffman-Taylor fingers, *Phys. Rev. A: At., Mol., Opt. Phys.*, 1988, **37**, 935–947.
29 H. Thomé, M. Rabaud, V. Hakim and Y. Couder, The Saffman-Taylor instability: From the linear to the circular geometry, *Phys. Fluids*, 1989, **1**, 224–240.
30 T. T. Al-Housseiny, P. A. Tsai and H. A. Stone, Control of interfacial instabilities using flow geometry, *Nat. Phys.*, 2012, **8**, 747–750.
31 E. O. Dias and J. A. Miranda, Control of radial fingering patterns: A weakly nonlinear approach, *Phys. Rev. E: Stat., Nonlinear, Soft Matter Phys.*, 2010, **81**, 016312.
32 Z. Zheng, H. Kim and H. A. Stone, Controlling viscous fingering using time-dependent strategies, *Phys. Rev. Lett.*, 2015, **115**, 174501.
33 S. Li, J. S. Lowengrub, J. Fontana and P. Palffy-Muhoray, Control of viscous fingering patterns in a radial Hele-Shaw cell, *Phys. Rev. Lett.*, 2009, **102**, 174501.
34 C. Y. Chen, C. W. Huang, L. C. Wang and J. A. Miranda, Controlling radial fingering patterns in miscible confined flows, *Phys. Rev. E: Stat., Nonlinear, Soft Matter Phys.*, 2010, **82**, 056308.
35 E. O. Dias, E. Alvarez-Lacalle, M. S. Carvalho and J. A. Miranda, Minimization of viscous fluid fingering: A variational scheme for optimal flow rates, *Phys. Rev. Lett.*, 2012, **109**, 144502.
36 D. Pihler-Puzovic, P. Illien, M. Heil and A. Juel, Suppression of complex fingerlike patterns at the interface between air and a viscous fluid by elastic membranes, *Phys. Rev. Lett.*, 2012, **108**, 074502.
37 D. Pihler-Puzović, R. Périllat, M. Russell, A. Juel and M. Heil, Modelling the suppression of viscous fingering in elastic-walled Hele-Shaw cells, *J. Fluid Mech.*, 2013, **731**, 162–183.
38 D. Pihler-Puzović, G. G. Peng, J. R. Lister, M. Heil and A. Juel, Viscous fingering in a radial elastic-walled Hele-Shaw cell, *J. Fluid Mech.*, 2018, **849**, 163–191.
39 B. Zhao, C. W. MacMinn and R. Juanes, Wettability control on multiphase flow in patterned microfluidics, *Proc. Natl. Acad. Sci. U. S. A.*, 2016, **113**, 10251–10256.
40 H. Tang, W. Grivas, D. Homentcovschi, J. Geer and T. Singler, Stability considerations associated with the meniscoid particle band at advancing interfaces in Hele-Shaw suspension flows, *Phys. Rev. Lett.*, 2000, **85**, 2112–2115.
41 A. Leshchiner, M. Thrasher, M. B. Mineev-Weinstein and H. L. Swinney, Harmonic moment dynamics in Laplacian growth, *Phys. Rev. E: Stat., Nonlinear, Soft Matter Phys.*, 2010, **81**, 016206.
42 A. De Wit and G. M. Homsy, Viscous fingering in reaction-diffusion systems, *J. Chem. Phys.*, 1999, **110**, 8663–8675.
43 Y. Nagatsu, K. Matsuda, Y. Kato and Y. Tada, Experimental study on miscible viscous fingering involving viscosity changes induced by variations in chemical species concentrations due to chemical reactions, *J. Fluid Mech.*, 2007, **571**, 475–493.
44 Y. Nagatsu, S. K. Bae, Y. Kato and Y. Tada, Miscible viscous fingering with a chemical reaction involving precipitation, *Phys. Rev. E: Stat., Nonlinear, Soft Matter Phys.*, 2008, **77**, 067302.
45 L. A. Riolfo, Y. Nagatsu, S. Iwata, R. Maes, P. M. J. Trevelyan and A. De Wit, Experimental evidence of reaction-driven miscible viscous fingering, *Phys. Rev. E: Stat., Nonlinear, Soft Matter Phys.*, 2012, **85**, 015304(R).
46 A. De Wit, Chemo-hydrodynamic patterns in porous media, *Philos. Trans. R. Soc., A*, 2016, **374**, 20150419.
47 D. M. Escala, A. De Wit, J. Carballido-Landeira and A. P. Munuzuri, Viscous Fingering Induced by a pH-Sensitive Clock Reaction, *Langmuir*, 2019, **35**, 4182–4188.
48 D. M. Escala, M. A. Budroni, J. Carballido-Landeira, A. De Wit and A. P. Muñuzuri, Self-organized traveling chemo-hydrodynamic fingers triggered by a chemical oscillator, *J. Phys. Chem. Lett.*, 2014, **5**, 413–418.
49 A. De Wit, Chemo-Hydrodynamic Patterns and Instabilities, *Annu. Rev. Fluid Mech.*, 2020, **52**, 531–555.
50 D. M. Escala and A. P. Muñuzuri, A bottom-up approach to construct or deconstruct a fluid instability, *Sci. Rep.*, 2021, **11**, 24368.
51 Y. Nagatsu, A. Hayashi, M. Ban, Y. Kato and Y. Tada, Spiral pattern in a radial displacement involving a reaction-producing gel, *Phys. Rev. E: Stat., Nonlinear, Soft Matter Phys.*, 2008, **78**, 026307.
52 S. M. Snyder, K. D. Cole and D. C. Sziag, Phase Compositions, Viscosities, and Densities for Aqueous Two-Phase Systems Composed of Polyethylene Glycol and Various Salts at 25 °C, *J. Chem. Eng. Data*, 1992, **37**, 268–274.
53 D. Molin and R. Mauri, Enhanced heat transport during phase separation of liquid binary mixtures, *Phys. Fluids*, 2007, **19**, 074102.
54 P. C. Hohenberg and B. I. Halperin, *Rev. Mod. Phys.*, 1977, **49**, 435–479.
55 L. Paterson, Radial fingering in a Hele Shaw cell, *J. Fluid Mech.*, 1981, **113**, 513–529.

56 J. A. Pojman, C. Whitmore, M. L. T. Liveri, R. Lombardo, J. Marszalek, R. Parker and B. Zoltowski, Evidence for the existence of an effective interfacial tension between miscible fluids: Isobutyric acid - Water and 1-butanol- water in a spinning-drop tensiometer, *Langmuir*, 2006, **22**, 2569–2577.

57 B. Zoltowski, Y. Chekanov, J. Masere, J. A. Pojman and V. Volpert, Evidence for the Existence of an Effective Interfacial Tension between Miscible Fluids. 2. Dodecyl Acrylate-Poly(dodecyl acrylate) in a Spinning Drop Tensiometer, *Langmuir*, 2007, **23**, 5522–5531.

58 D. Jasnow and J. Viñals, Coarse-grained description of thermo-capillary flow, *Phys. Fluids*, 1996, **8**, 660–669.

59 N. Vladimirova, A. Malagoli and R. Mauri, Two-dimensional model of phase segregation in liquid binary mixtures, *Phys. Rev. E: Stat. Phys., Plasmas, Fluids, Relat. Interdiscip. Top.*, 1999, **60**, 6968–6977.

60 R. Mauri, R. Shinnar and G. Triantafyllou, Spinodal decomposition in binary mixtures, *Phys. Rev. E: Stat. Phys., Plasmas, Fluids, Relat. Interdiscip. Top.*, 1996, **53**, 2613–2623.

61 B. Vonnegut, Rotating bubble method for the determination of surface and interfacial tensions, *Rev. Sci. Instrum.*, 1942, **13**, 6–9.

62 Y. Nagatsu and T. Ueda, Effects of reactant concentrations on reactive miscible viscous fingering, *AIChE J.*, 2001, **47**, 1711–1720.

63 I. Bischofberger, R. Ramachandran and S. R. Nagel, Fingering versus stability in the limit of zero interfacial tension, *Nat. Commun.*, 2014, **5**, 5265.

64 P. Bunton, D. Marin, S. Stewart, E. Meiburg and A. De Wit, Schlieren imaging of viscous fingering in a horizontal Hele-Shaw cell, *Exp. Fluids*, 2016, **57**, 28.

65 P. Bunton, B. Dice, J. A. Pojman, A. De Wit and F. Brau, Reconstruction by fluorescence imaging of the spatio-temporal evolution of the viscosity field in Hele-Shaw flows, *Phys. Fluids*, 2014, **26**, 114106.

66 F. Haudin, L. A. Riolfo, B. Knaepen, G. M. Homsy and A. De Wit, Experimental study of a buoyancy-driven instability of a miscible horizontal displacement in a Hele-Shaw cell, *Phys. Fluids*, 2014, **26**, 044102.